Model of the development of a sedimentary basin of the pull-apart type

Article *in* Doklady Earth Sciences · September 2001

CITATIONS
9

READS
49

2 authors, including:

Oleg Petrovich Polyansky
Sobolev Institute of Geology and Mineralogy
99 PUBLICATIONS **668** CITATIONS

SEE PROFILE

Doklady Earth Sciences, Vol. 380, No. 7, 2001, pp. 800–805. Translated from Doklady Akademii Nauk, Vol. 380, No. 3, 2001, pp. 368–373.

GEOLOGY

Model of the Development of a Sedimentary Basin of the Pull-Apart Type

O. P. Polyansky and Academician of the RAS N. L. Dobretsov

Received June 4, 2001

Strike-slip rifts or basins of the pull-apart type are produced by extension of the Earth's crust in the presence of two or more fractures that are nearly parallel but shifted relative to each other. Depending on the value of displacement between fractures, the basin can possess a rhomb- or parallelogram-shaped form. Typical examples of such structures are the Kurai and Chuya depressions in the Gornyi Altai region [1], the Tunka Depression and other intermontane troughs in the Baikal Rift Zone [2], and basins of the Dead Sea [3, 4] and the Salton Trough at the extension of the San Andreas Fracture Zone, California [5].

Pull-apart mechanisms are insufficiently well studied to date. Deformations of elastic medium during a simple strike-slip displacement between two parallel fractures are described in [3, 6]. In [3], the model profile across the Dead Sea depicts a graben with maximal subsidence of the basement sandwiched between fractures to a depth of 400–600 m. In [6], the maximal subsidence of basin does not exceed 100 m at different values of parameters of the elastic lithosphere (Poisson's ratio and Young's modulus) and external stress. The main inconsistency of models of the elastic lithosphere relative to real structures lies in the fact that vertical displacements in the models do not exceed ±0.5 km, while the depth of sedimentary basins of this type reaches 5–10 km [4, 7]. In order to construct a model of lithospheric deformations and the stressed state leading to the development of basins of the pull-apart type, we modified the PLATES program [8] that realizes the 2.5-D approximation for solving 3-D problems. The applicability of this approach for recent deformations corresponding to the rapid stage of the Baikal Rift formation is demonstrated in [9].

The model is based on the following major assumptions. Owing to the presence of an irregular network of fractures, curvilinear boundaries of plates, and intricate deep structure of crust and mantle, the problem formulated in this work represents an essentially 3-D model. In addition, we have to consider stationary deformations that are likely to be unaltered during tectonic activity. In other words, the model does not take into consideration short-term elastic dislocations, and the entire deformation is assumed to be a continuous inelastic process. We use the approximation of problem pertaining to the deformation of two thin plates (crust/mantle) that can jointly deform depending on rheological properties of the crust and upper mantle. The state of equilibrium in a stressed medium with negligible inertial terms is accepted as the equation of motion:

$$\frac{\partial \sigma_{ij}}{\partial x_j} + \rho g_i = 0. \quad (1)$$

Vertical components of stresses are governed by the condition of isostasy. We use the Boussinesq approximation pertaining to incompressibility in the equation of mass conservation

$$\nabla \cdot U = 0. \quad (2)$$

The equation of heat conductivity neglects nonstationary and convective terms along with the lateral heat transfer. Thermophysical properties of the crust and lithospheric mantle are assumed to be different. The temperature value is found from the analytical solution related to heat propagation in a two-layer lithosphere:

$$T_n(z) = T_s + \frac{(Q + h_n H_n)z}{K_n} - \frac{H_n z^2}{2K_n}, \quad (3)$$

where $n = \{1, 2\}$ corresponds to the crust and mantle, z is the vertical coordinate in a layer, and h_n is the layer thickness. Other values of parameters in the above equations are given in the table.

Rheology. The applied method admits the existence of three types of rheological behavior of material. In the upper section of crustal and mantle layers, brittle rheology obeys the Coulomb–Mohr's law of friction:

$$\sigma_s^{\text{friction}} = f \cdot (\sigma_n - \text{Bi} \cdot P_p) + \sigma_c. \quad (4)$$

The value of the friction coefficient f in Eq. (4) is differently prescribed for existing fracture surfaces and

United Institute of Geology, Geophysics, and Mineralogy (UIGGM), Siberian Division, Russian Academy of Sciences, pr. akademika Koptyuga 3, Novosibirsk, 630090 Russia

Table

Parameter	Crust	Mantle	Formula
Coefficient of fracture friction, f_f	0.17	–	(4)
Coefficient of medium friction, f_m	0.85	0.85	
Biocoefficient, Bi	1.0	1.0	
Coefficient of cohesion, σ_a	0.0	0.0	
Preexponential viscosity constant, A (Pa · s$^{1/n}$)	$2.3 \cdot 10^9$	$5.4 \cdot 10^6$	(5)
(Activation energy)/nR, B (K)	$4.0 \cdot 10^3$	$1.8 \cdot 10^4$	
Exponent, n	3	3	
(Activation volume)/nR, C (K/Pa)	0	0.017	
Heat conductivity, K (J/(m · s · K))	3.0	4.06	(3)
Radioactivity, H (J/(m^3 · s))	$4.5 \cdot 10^{-7}$	$3.2 \cdot 10^{-8}$	
Heat flow, Q_s (mW/m^2)	50	–	
Yield limit, σ_{yield} (MPa)	500	500	(6)
Density, ρ_0 (kg/m^3)	2800	3330	(9)
Thermal expansion, α (K^{-1})	$2.4 \cdot 10^{-5}$	$3.1 \cdot 10^{-5}$	
Shear rate (cm/yr)	0.5–5		Boundary conditions
Compression rate (cm/yr)			

medium volume. Viscous rheology is described as a temperature-dependent nonlinear creep:

$$\sigma_s^{cr} = A \cdot [2\sqrt{II}]^{1/n-1} \exp\left(\frac{B + C_z}{T}\right) \cdot \dot{e}_s^{cr}, \quad (5)$$

where II depicts the second invariant of the strain rate tensor. An ideal plasticity obeys the Tresque law for maximal shear stress:

$$\sigma^{plast} \le \sigma_{yield}. \quad (6)$$

The depth of transition from brittle deformation to viscous-plastic deformation is a function of the local geotherm, strain rate, and stress state form. Therefore, it is governed by the condition of equality of differential stresses under the brittle and viscous-plastic rheology in the crust and upper mantle. The resultant stress at a specified depth will be minimal among the possible values:

$$\sigma_s = \inf(\sigma_s^{frict}, \sigma_s^{cr}, \sigma_s^{plast}). \quad (7)$$

Parameters of the model, their variation ranges, and dimensional units for the crust and mantle are given in the table. It is supposed that the crustal layer is governed by properties of dry granite, while the lithospheric mantle is characterized by properties of dunite. Experimental estimates of rheological parameters for quartz-dominated rocks of the crust and olivine-bearing rocks of the mantle are reported in [10]. It has been experimentally proven that the heated lower mantle is deformed by the mechanism of creep. By analogy with the Newton liquid viscosity, the effective viscosity of a nonlinear liquid can be obtained on the basis of Eq. (5):

$$\eta = \frac{\sigma}{2\dot{\varepsilon}} = A \cdot [II]^{(n-1)/2n} \exp\left(\frac{E}{nRT}\right). \quad (8)$$

The standard expression

$$\rho = \rho_0(1 - \alpha\Delta T), \quad (9)$$

which completes the system description, was used as an equation of state.

The impact of effective viscosity upon the joint deformation of crust and mantle was accomplished in [9] by searching values of rheological constants A, n, and activation energy $E/nR = B + C_z$ in the exponential law (5) and values of friction coefficient f from Eq. (4) for fractures. Parameters of the crust and mantle were chosen among the available laboratory data and estimates of some geological settings, such as the San Andreas Fracture Zone [8] and accretionary complexes of Asia [11].

Results. The model area encompasses the shear deformation zone, 600 × 600 × 200 km in size (along x, y, and z coordinates). The irregular grid of finite elements is composed of triangular elements of continuum and curvilinear elements of fractures. The grid is adjusted for the introduction of two parallel fractures that are reactivated during tectonic processes. The dip of fractures was set at 25°, 65°, and 90° in different versions of the model. In order to simplify the model, the Moho boundary surface was accepted as a flat plane at the crustal thickness of 30 km. The lithosphere thickness was 200 km for platformal regions, 100 km for rift

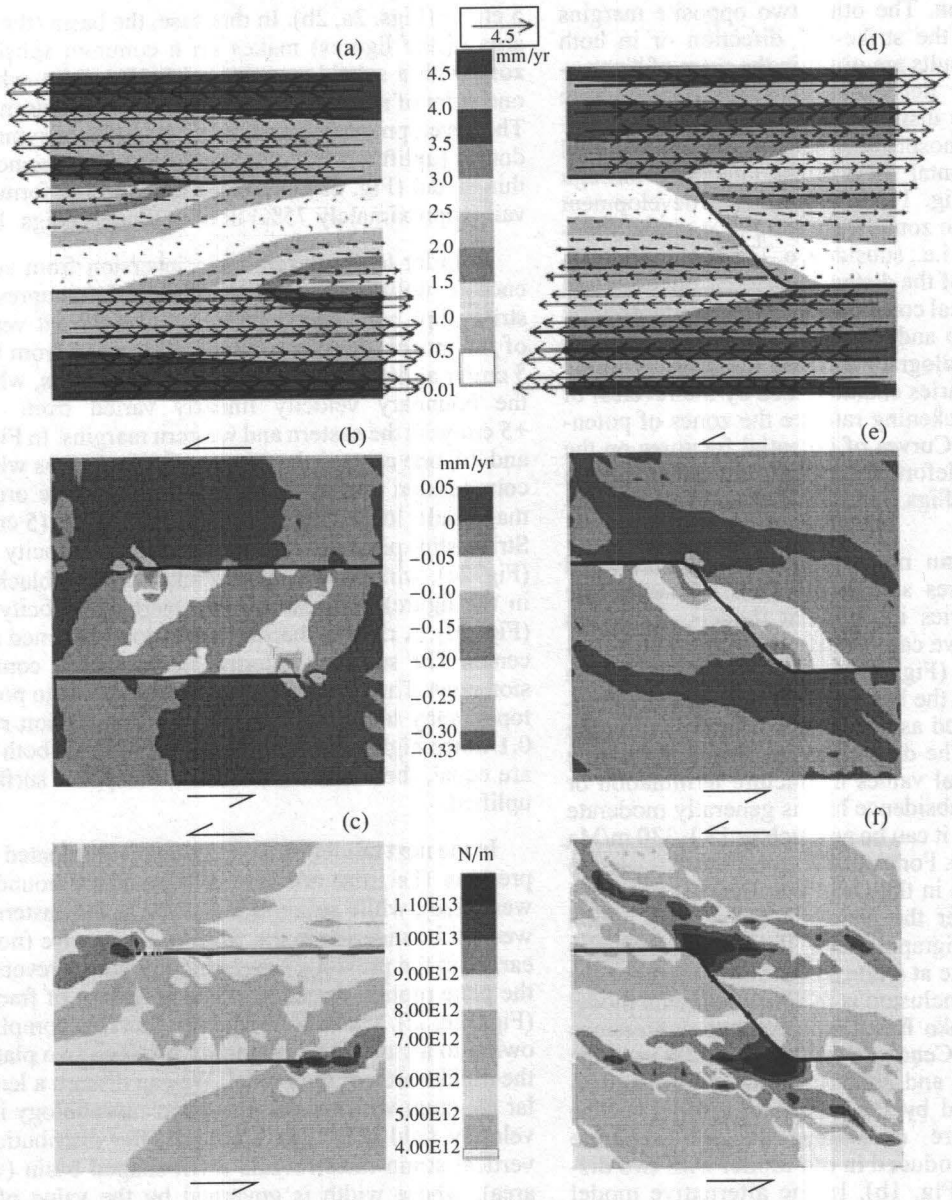

Fig. 1. Model calculations of velocity fields (a, d), thinning/thickening of lithosphere (b, e), and stress (c, f). Bold lines show fractures. (1a–1c) Models with two parallel (disjoint) fractures; (1d–1f) models with a Z-shaped fracture. In Figs. 1b and 1e, the basin formation (lithosphere subsidence) area is shown by light shades, while the lithosphere uplift field is shown by dark gray shades. In Figs. 1c and 1f, maximal shear stress zones are shown by dark gray shades.

zones, or constant. The conductive (vertical) heat transfer was assumed to be dominant in order to take into account the temperature dependence of rheology. The surface heat flux of 50 mW/m^2 was accepted as the boundary condition.

In order to investigate the topography dynamics related to viscous flows in the underlying mantle, we modeled tectonic settings of horizontal strike-slip along with joint compression and strike-slip. We carried out numerous tests with different boundary conditions and rheological constants. We present here only those results that can most adequately explain the development of basins of the pull-apart type.

Figure 1 shows results pertaining to the model of basin development between two parallel (disjoint) fractures (Figs. 1a–1c) and near a Z-shaped fracture (Figs. 1d–1f). The shear rate of 5 mm/yr at the northern and southern margins of the field was accepted as the

boundary condition. The other two opposite margins remained free in the strike-slip direction or in both directions. The results are given in the form of "instantaneous" velocity fields on the lithosphere surface (Figs. 1a, 1d), the distribution of the thickening/thinning rate of the lithosphere (Figs. 1b, 1e), and the total sum of the horizontal shear stress integrated through the lithosphere (Fig. 1c, 1f). The basin development field corresponds to zones with a negative rate of lithosphere thickening, i.e., subsidence. The basin morphology is a function of the distance between fractures and their dip, rheological constants of crust and lithospheric mantle. Figures 1b and 1e demonstrate that the basin resembles a parallelogram inclined in accord with the strike-slip. Boundaries characterized by the reversal of the lithosphere thickening rate are the zones of potential normal faults. Curves of potential fractures on the figures of shear deformations are extensions of the existing fractures (Figs. 1c, 1f) and are traced by maximal stress zones.

The model basin morphology fits rhomb-shaped geological structures sufficiently well. However, the deep structure varies in different models. Based on modeling results, we can identify basins with two separate depressions (Fig. 1b) or a single subsidence region (Fig. 1e). In the latter model, the resultant structure can be qualified as a graben-in-graben within the strike-slip basin. The depth of such basins is variable and attains maximal values in fracture termination or bend zones. The subsidence rate is generally moderate (30–50 m/Ma), but it can be as much as 180–330 m/Ma in strike-slip basins. For example, subsidence related to shear deformations in the Dead Sea Basin is not more than 66 m/Ma over the Neogene–Quaternary period [2]. Based on stratigraphic data, the Tunka strike-slip rift began to subside at a rate of 70–90 m/Ma since the Oligocene. This conclusion is in agreement with model estimates. The Tunka Basin includes two depressions that are filled with Cenozoic sediments (2200 m in the western depression and 2800 m in the eastern depression) and separated by the basement uplift [7]. The pull-apart structure consisting of two separate depressions is reproduced in our model with two displaced fractures (Fig. 1b). In the alternative model with a Z-shaped fracture, one can see two narrow ridges that are extended along fractures (rift flanks) that delineate the basin.

Model estimates of the mean subsidence rate (100 m/Ma) obtained for the Salton Basin related to strike-slip faults are one order of magnitude lower than the real values registered in this structure. The maximal sedimentation rate in the Imperial Valley within the Salton Basin is as much as 1100 m/Ma (5500 m/5 Ma) [3]. It is worth mentioning that the horizontal strike-slip rate of the Pacific Plate relative to the North American Plate is 22 mm/yr [12], which is also one order of magnitude higher relative to the GPS data on the Tunka Basin [13]. In order to model a rapidly subsiding basin, we performed calculations with a strike-slip rate of 5 cm/yr (Figs. 2a, 2b). In this case, the basin (the white area in the figures) makes up a common subsidence zone with a subsidence rate of 5–10 mm/yr, which is one order of magnitude higher than in previous models. The development of one depression and four symmetric domes (uplifts) is a typical feature of displacements in this model (Fig. 2b). Negative topographic forms prevail (approximately 75%) in both models (Figs. 1, 2).

In order to study the basin inversion from subsidence to uplift, we applied combined (compression–strike-slip) boundary conditions. In different versions of the model, the compression rate varied from 0.5 to 5 cm/yr at the northern and southern margins, whereas the boundary velocity linearly varied from –5 to +5 cm/yr at the eastern and western margins. In Figs. 2c and 2d, one can see the results of calculations with the compression rate of 0.5 cm/yr, which is one order of magnitude lower than the strike-slip rate (5 cm/yr). Strike-slip prevails in the horizontal velocity field (Fig. 2c), while lithosphere thickening (the black area in the figure) dominates in the vertical velocity field (Fig. 2d). A rhomb-shaped depression is formed at the center. The subsidence terminates at higher compression rates. Thus, inversion from the negative to positive topography takes place when the compression rate is 0.1 times higher than the strike-slip rate. If both rates are equal, the entire area of the lithosphere surface is uplifted.

In the next model version, we again eliminated compression (i.e., the northern and southern boundaries were free), while strike-slip was set at the eastern and western boundaries in the form of a stepwise (not linear, as in the previous case) function with a reversal of the plate motion direction at the boundary of fractures (Figs. 2e, 2f). The east–west extension is accomplished owing to a curvilinear boundary between two plates in the middle area of the model. We can discern a lenticular structure with typical pull-apart morphology in the velocity field (Fig. 2e). However, the distribution of vertical strain rates reveals a rift-shaped basin (white area), whose width is governed by the value of displacement between fractures. The model shows that the plate motion direction at the boundary of basins should change in a continuous rather than stepwise manner for the development of strike-slip basins.

The comparison of model results with geological data suggests that basins of the pull-apart type are a specific form of sedimentary basins that are only formed in certain geodynamic settings. Such structures are developed in a strike-slip zone that makes up the transform boundary between two plates (e.g., Siberian–Mongolian, African–Arabian, and Pacific–North American plates). The basin structure is a function of the geometry of fractures, strike-slip and compression rates, and rheological properties of the lithosphere.

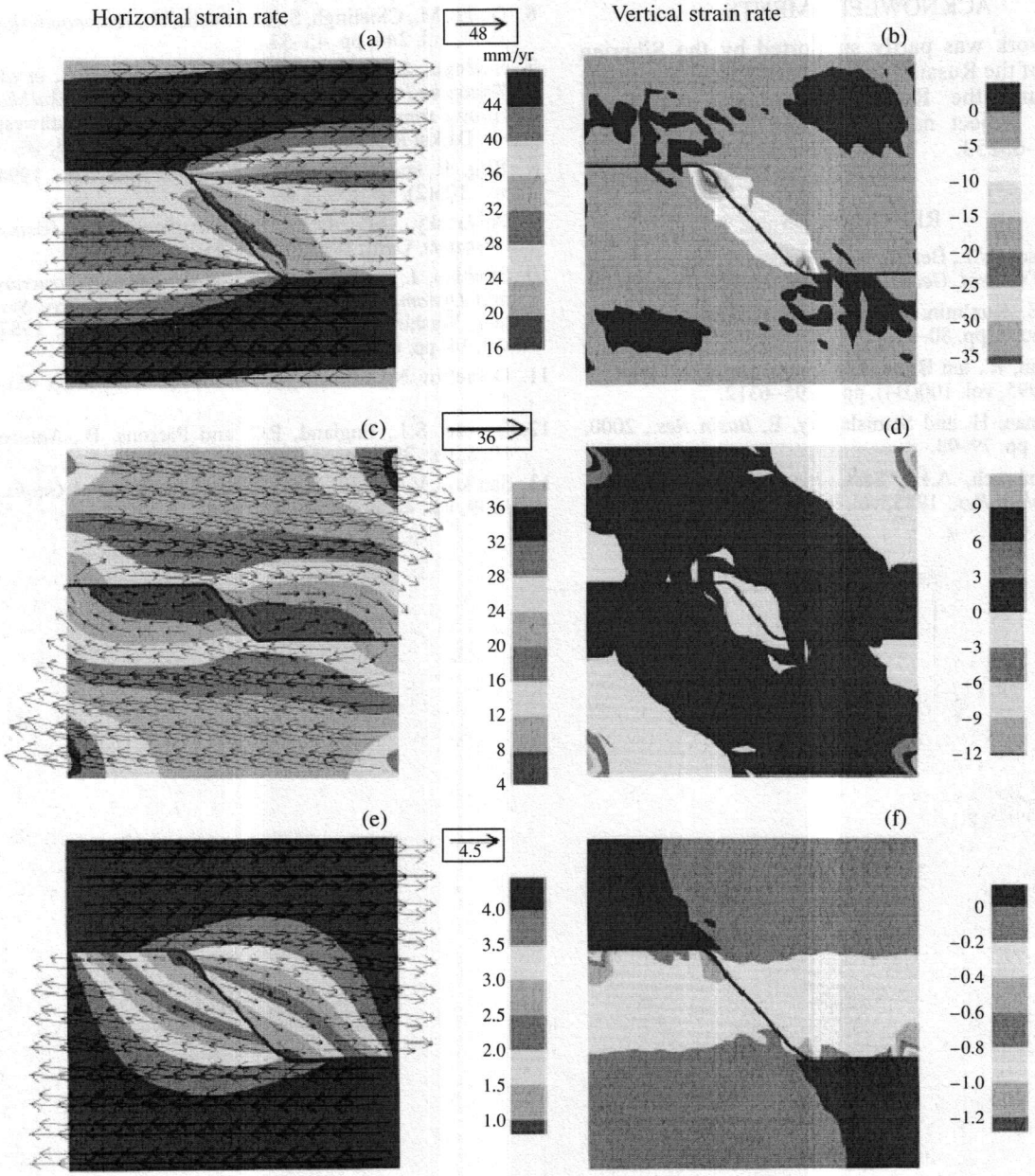

Fig. 2. (a, b) Model of shear deformation at a rate of 5 cm/yr. The basin (light shade) represents a single field subsiding at a rate of 5–10 mm/yr. Local maximums of subsidence rate are registered near fracture bends (b). (c, d) Model of simultaneous dextral (W–E) shear deformation at a rate of 4 cm/yr and N–S compression at a rate of 5 mm/yr (one order of magnitude lower). Strike-slip dominates in the field of horizontal velocity (c), while lithosphere thickening (dark shade) prevails in the field of vertical velocity (d). A rhomb-shaped basin is formed at the field center. Local anomalies at the corners are produced by the impact of diverse boundary conditions at adjacent (compression–strike-slip) boundaries. (e, f) Model of shear deformation with free northern and southern boundaries: (e) velocity is governed by a stepwise function with orientation reversal at the eastern and western boundaries, (f) the basin (light shade) is formed as a rift governed by the value of shift between fractures. The gray shade depicts low subsidence rate (0–0.2 mm/yr), while the dark shade shows uplift.

ACKNOWLEDGMENTS

This work was partly supported by the Siberian Division of the Russian Academy of Sciences, project no. 30 and the Russian Foundation for Basic Research, project nos. 99-05-64677, 99-05-64727, and 01-05-65253.

REFERENCES

1. Dobretsov, N.L, Berzin, N.A., Buslov, M.M. and Ermakov, V.D., *Geol. Geofiz.*, 1995, vol. 36, no. 10, pp. 5–19.
2. Balla, Z., Kuz'min, M.I., and Levi, K.G., *Geotektonika,* 1990, no. 2, pp. 80–91.
3. Katzman, R., ten Brink, U.S., and Lin, J., *J. Geophys. Res.*, 1995, vol. 100(B4), pp. 6295–6312.
4. Gvirtzman, H. and Stanislavsky, E, *Basin Res.*, 2000, vol. 12, pp. 79–93.
5. Lanchenbruch, A.H., Sass, J.H., and Galanis, S.P., *J. Geophys. Res.,* 1985, vol. 90(B8), pp. 6709–6736.
6. Golke, M., Cloetingh, S., and Fuchs, K., *Tectonophysics*, 1994, vol. 240, pp. 45–57.
7. Sherman, S.I., Medvedev, M.E., Ruzhich, V.V., *et al.*, *Tektonika i vulkanizm yugo-zapadnoi chasti Baikal'skoi riftovoi zony* (Tectonics and Volcanism in the Southwestern Baikal Rift Zone), Novosibirsk: Nauka, 1973.
8. Birg, P. and Kong, X., *Bull. Geol. Soc. Am.*, 1994, vol. 106(2), pp. 159–174.
9. Polyansky, O.P., *Active Tectonic Continental Basins: Abstracts,* Gent, 1998, pp. 94–95.
10. Strehlau, J. and Meissner, R., *Compositions, Structure and Dynamics of the Lithosphere-Asthenosphere System*, Washington, D.C.: Am. Geophys. Union, 1987, vol. 16, pp. 69–87.
11. Dobretsov, N.L, *Petrologiya,* 2000, vol. 8, no. 6, pp. 451–476.
12. Bourne, S.J., England, P.C. and Parsons, B., *Nature*, 1998, vol. 391, pp. 655–659.
13. San'kov, V.A., Levi, K.G., Kale, E., *et al.*, *Geol. Geofiz.*, 1999, vol. 40, no. 3, pp. 422–430.